J. Ocean Univ. China (Oceanic and Coastal Sea Research)
https://doi.org/10.1007/s11802-025-6023-8
ISSN 1672-5182, 2025 24 (4): 1017-1026
http://www.ouc.edu.cn/xbywb/
E-mail:xbywb@ouc.edu.cn

The Effect of Triethanolamine Dodecylbenzene Sulfonate on Metastable Corrosion of 304 Stainless Steel

LIAO Yingdi[1), 3)], ZHANG Huan[2), 1)], WANG Xin[1)], CHEN Li[1)], HUANG Chenggeng[1)], ZHAO Yazhou[1)], and DA Bo[1), 3), *]

1) *College of Harbour, Coastal and Offshore Engineering, Hohai University, Nanjing* 210098, *China*
2) *Chongqing Xike Water Transport Engineering Consulting Co., Ltd., Chongqing* 402247, *China*
3) *Key Laboratory of Coastal Disaster and Defence of Ministry of Education, Hohai University, Nanjing* 210098, *China*

(Received September 3, 2024; revised March 21, 2025; accepted March 29, 2025)

Abstract Reinforcing bars in concrete structures in marine environment are prone to pitting corrosion, which threatens the safety of engineering structures. In order to effectively mitigate the pitting corrosion of reinforcing bars, the electrochemical testing and atomic force microscopy are adopted, the effect of triethanolamine dodecylbenzene sulfonate (TDS) on metastable pitting behavior of 304 stainless steel (304 SS) in simulated concrete pore solutions (SCPS) with chlorine contamination was studied. The results show that the corrosion potential (E_{corr}) and breakdown potential (E_b) increased with the growth of the TDS concentrations. Statistical characteristics of metastable pits suggested that as the TDS concentrations increased in the SCPS, the parameters were all decreased. The Mott-Schottky tests exhibited that, although the donor density (N_D) diminished, the thickness of the space charge layer (W) increased with increasing TDS concentrations. Investigation results showed that TDS inhibited the sprouting and growth of metastable pits, and with greater TDS concentration, it becomes more difficult for metastable pits to transfer into stable pits in the SCPS, the generated stable passive film prevented the sprouting of pitting corrosion, It is recommended to use TDS with a concentration of not less than 3.364×10^{-4} mol/L in engineering, so that the sensitivity of passivation film of 304SS to chloride erosion is reduced.

Key words ocean engineering; 304 stainless steel; TDS; metastable pits; passive film

1 Introduction

In the ocean engineering, the most widespread form of construction material is reinforced concrete where passive film normally forms on the embedded rebar due to the high alkaline concrete environment (Chen *et al*., 2019). However, pitting corrosion happens as a consequence of carbonation and the penetration of chlorine ions, which induces the destruction of passivation and the subsequent pitting on steel surfaces (Da *et al*., 2016). Prior to the formation of stable pits, nucleation and expansion of metastable pits happens on the materials surfaces. If the growth rate of pits is relatively slow, repassivation would happen, while the metastable pits would transfer into the stable pits when the outward diffusion process is fast enough (Zhao *et al*., 2023). Once the stable pits are formed, the corrosion process is speeded up which actually may bring a threat to the safety of the service concrete structures. More importantly, due to its difficulty in identifying and foreknowing, pitting corrosion poses a greater danger and harm than general corrosion (Abass *et al*., 2018). Consequently, the investigation on the stages of nucleation, propagation, and repassivation is conducive to predict the safety and lifetime of the concrete structure (Liao *et al*., 2022).

To minimize the transition probability of metastable pits, the inhibition mechanisms of some inorganic inhibitors have been investigated. Naghizadeh *et al*. (2015) reported that $Cr_2O_7^{2-}$ increased the resistance to pitting corrosion on 316SS surface as the establishment of stable pit was decreased, the dissolution rate of species inside the pit cavities was reduced, and the survival probability for the pit generation was noticeably increased as well. Haleem *et al*. (2010) discovered that the passive films tend to heal and thicken with the concentrations of some anions, and at the identical concentration of these anions, it is observed that their resistance to pitting corrosion deceases as follows: $MoO_4^{2-}>WO_4^{2-}>NO_2^->HPO_4^{2-}>CrO_4^{2-}$. Dong *et al*. (2011) compared the impact between nitrite and tetraethylenepenotamine (TEPA) on the pitting susceptibility of passive film and found that nitrite increased the pitting potential and rehabilitated the metastable pits more efficient than TEPA.

Through the inorganic inhibitors are relatively efficient in inhibiting pitting corrosion, the toxicity can also pose a risk to environment and human health. Some environment-friendly organic inhibitors have attracted researcher'

* Corresponding author. E-mail: dabo@hhu.edu.cn

s attention and were applied in engineering implementation in the past decades. Zhao *et al*. (2019) confirmed through optical observation of carbon steel surface that triethanolamine dodecylbenzene sulfonate (TDS) significantly inhibited pitting and improved the corrosion resistance of Q235 carbon steel in pore solution. The TDS adsorption film on the steel surface blocks the active sites from the chloride ions, playing a dominant role in suppressing the corrosion initiation. Yet the effect of TDS concentration on pitting resistance of reinforcement remains unclear. Thus, the inhibition performance of TDS concentrations on the transformation of metastable pit was investigated from a statistical perspective in this work.

2 Experiment and Methods

2.1 Experimental Solutions and Materials

To imitate the concrete environment after contamination by chlorine ions, the simulated concrete pore solution (SCPS) was manufactured, containing 0.06 mol/L KOH, 0.2 mol/L NaOH, 0.01 mol/L $Ca(OH)_2$, 0.24 mol/L $NaHCO_3$, and 0.25 mol/L NaCl. The initial pH of the SCPS was 12.5, measured by a Leici pH meter (PHS-3E) calibrated with three standard buffer solutions. The corrosion inhibitor, triethanolamine dodecylbenzene sulfonate (TDS), was sourced from Guangzhou Dongxing Previous Chemical Co., China. All the experimental solutions were made up with reagents of analytical grade and deionized water, with TDS concentrations of 0, 0.841×10^{-4}, 1.682×10^{-4} and 3.364×10^{-4} mol/L. The molecular structure of TDS is shown in Fig.1.

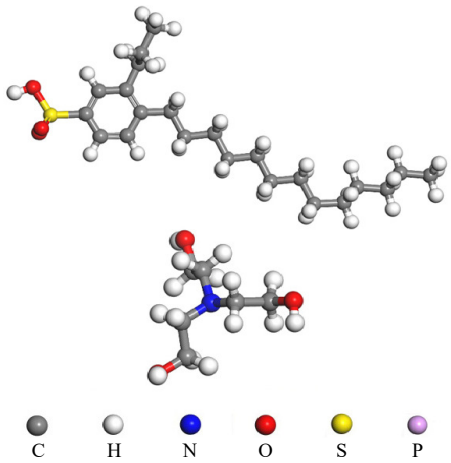

Fig.1 Molecular structure of triethanolamine dodecylbenzene sulfonate.

Cylindrical specimens of 1 cm in length and 1 cm in diameter were cut from 304SS bars, and their chemical composition (wt.%) is: Fe 60.82, Cr 18, Ni 14, Cu 4, Mn 2, Si 1, C 0.1, P 0.05 and S 0.03. These specimens were polished with the sand paper of 240-400-800-1200-1500-2000 grades, and rinsed with the alcohol to degrease prior to performing electrochemical measurements. All specimens were encapsulated with epoxy resin, and 0.79 cm^2 working area of the electrode was exposed.

2.2 Electrochemical Measurements

The statistical characteristics of metastable pits and the performance of passive film were investigated using potentiodynamic polarization, potentiostatic polarization and Mott-Schottky test. All electrochemical measurements were duplicated thrice under the identical conditions and the middle one was used as a representation.

The electrochemical experiments were made by using a Wuhan Corretest CS350 workstation equipped with a three-electrode system using a saturated calomel electrode (SCE) as the reference electrode, and a platinum electrode as the counter electrode. The three-electrode system is shown in Fig.2.

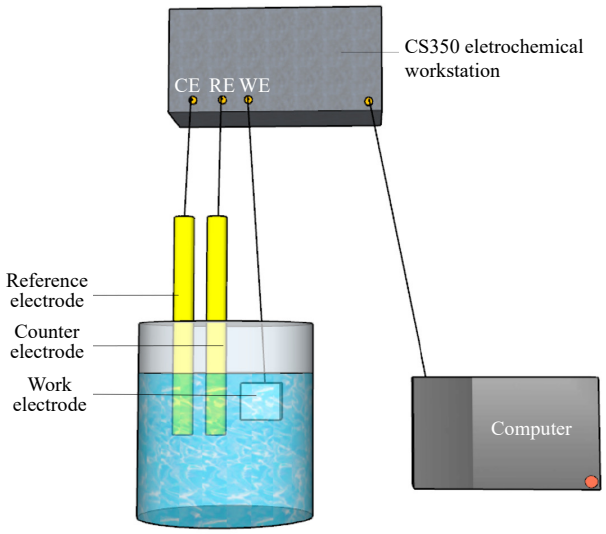

Fig.2 Three-electrode system.

The potentiodynamic polarizing sweep was carried out with 0.2 mV/s ranging from −0.3 V to 1.5 V versus the open circuit potential (Yang *et al*., 2017). If stable pits appeared on the surface of specimens before the potential reached to a set value, the potentiodynamic polarization was stopped in advance. Depending on the experimental findings of the potentiodynamic polarization, the potentiostatic polarizations were performed at a potential of 0.3 V, related to V_{SCE}. The current transients were recorded at 5 Hz frequency using potentiostatic polarizations, and each potentiostatic polarization lasted 360 min.

As a means of analyzing passive film characterizations of 304SS immersed in the SCPS, Mott-Schottky tests were conducted at 1000 Hz frequency with 0.05 V potential increments, ranging from −1.5 V_{SCE} to 1.0 V_{SCE}.

2.3 AFM Observations

After the potentiostatic polarization, the samples were ultrasonically cleaned for 3 min, then flushed it well with distilled water, and then dried in a vacuum drying oven. An atomic force microscopy (AFM Park system) was used to capture the images of pits on the 304SS and assessed the impact of TDS concentrations on the morphology of metastable pits. The scan rate of the nanoprobe

cantilever was kept constant at 1 Hz in an area of 10 μm× 10 μm under the tapping mode. Finally, the Gwyddion software was utilized to obtain the 3D morphology and depth of the metastable corrosion pits.

3 Results and Discussions

3.1 Potentiodynamic Measurement

The potentiodynamic polarization curves of 304SS in the SCPS with different TDS concentrations are presented in Fig.3. The polarization curve has a broadly passive range, and then the breakdown potential (E_b) occurs when the current density rises dramatically. The corrosion potential (E_{corr}) can be acquired by fitting the potentiodynamic polarization data with Cview 2 software, similarly, the corrosion current density (i_{corr}) is calculated. The corrosion inhibition efficiency (η) was calculated as described below.

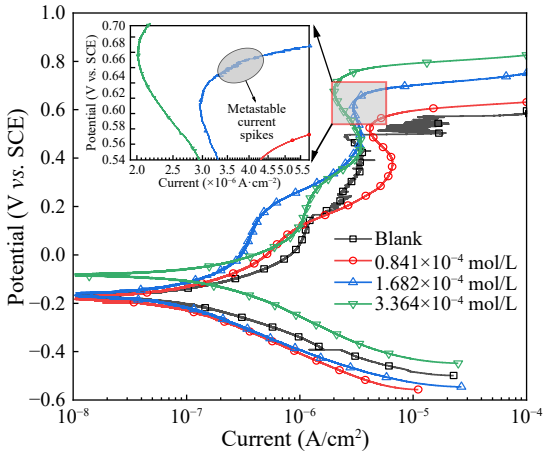

Fig.3 Potentiodynamic polarization curves of 304SS in the SCPS with different TDS concentrations.

$$IE = \frac{I^0_{corr} - I'_{corr}}{I^0_{corr}} \times 100\%, \quad (1)$$

where I'_{corr} and I^0_{corr} stand for the corrosion current density of 304SS in the existence and absence of TDS in the SCPS, respectively.

Determined the corrosion kinetic parameters of 304SS are listed in Table 1. It was clear that E_b increased with increasing TDS concentrations, which indicated that the passive film became much denser and it was less susceptible to the attack of chloride. Meanwhile, E_{corr} increased from −0.19 V_{SCE} to −0.08 V_{SCE}, and the *IE* increased to 59.6% when the TDS concentration increased to 3.364×10^{-4} mol/L. The enhancement of E_{corr} is ascribed to the either the suppression of anodic reaction or promotion of cathodic reaction (Wang *et al.*, 2020). The polarization curves in Fig.3 suggested that the polarization rate in anodic region increases while that in the cathodic remains almost constant. This indicates that TDS is an anode-type corrosion inhibitor (Zhang and Long, 2010).

Table 1 The corrosion kinetic parameters of 304SS in the SCPS with different TDS concentrations

Concentration (mol/L)	E_{corr} (V *vs.* SCE)	i_{corr} (A/cm²)	E_b (V *vs.* SCE)	*IE*
–	−0.175	5.527×10^{-6}	0.500	–
0.841×10^{-4}	−0.169	3.582×10^{-6}	0.552	35.2%
1.682×10^{-4}	−0.167	2.965×10^{-6}	0.653	46.4%
3.364×10^{-4}	−0.078	2.219×10^{-5}	0.736	59.6%

3.2 Potentiostatic Measurement

Figure 4 presents a typical current peak of metastable pit on the specimen in the SCPS with 1.682×10^{-4} mol/L TDS. A current fluctuation over 0.02 is defined as an individual metastable pit (Lu *et al.*, 2019). The parameters are defined as follows: i_{bg} is the background current, which can be obtained by smoothing the current density with Origin software, i_{max} is the maximum value of the current density, i_{peak} is the gap between i_{max} and i_{bg}. t_0 is the time when metastable pit starts to grow and the repassivation ends in t_2. t_1 is the time related to the maximum current density (i_{max}). The growth and repassivation time (t_{grow} and t_{rep}) of metastable pit are specified as t_1 minus t_0, t_2 minus t_1, respectively, the lifetime of a metastable pit is t_2 minus t_0 (Feng *et al.*, 2016). Based on the above parameters, the growth and repassivation rate (K_{grow} and K_{rep}) were defined as (Tian *et al.*, 2021):

$$K_{grow} = \frac{i_{peak}}{t_{grow}} = \frac{i_{peak}}{t_1 - t_0}, \quad (2)$$

$$K_{rep} = \frac{i_{peak}}{t_{rep}} = \frac{i_{peak}}{t_2 - t_1}. \quad (3)$$

A typical current transient is shown in Fig.5 for 304SS in the SCPS with different TDS concentrations. The test time of the potentiostatic polarization is so long that the metastable pitting of the current peak and signal noise seem to be indistinguishable. To highlight the difference between metastable current peak and signal noise, we enlarged the local data of potentiostatic polarization, and the metastable current peak and signal noise. In the specimens, the current density decreased sharply at first and then stabilized. The rapid drop in current density was a result of the passive film. The formation rate and dissolution rate of the passive film are balanced within the work-

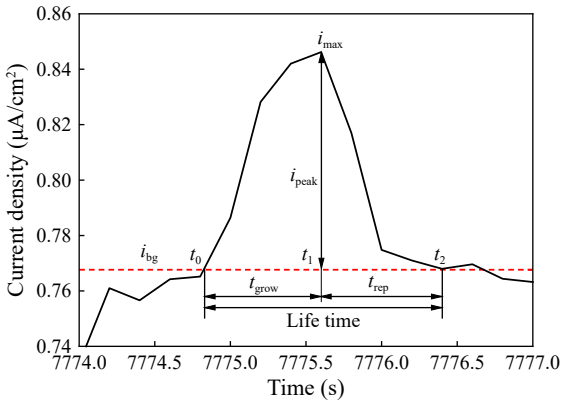

Fig.4 Typical current peak of specimen in the SCPS with 1.682×10^{-4} mol/L TDS.

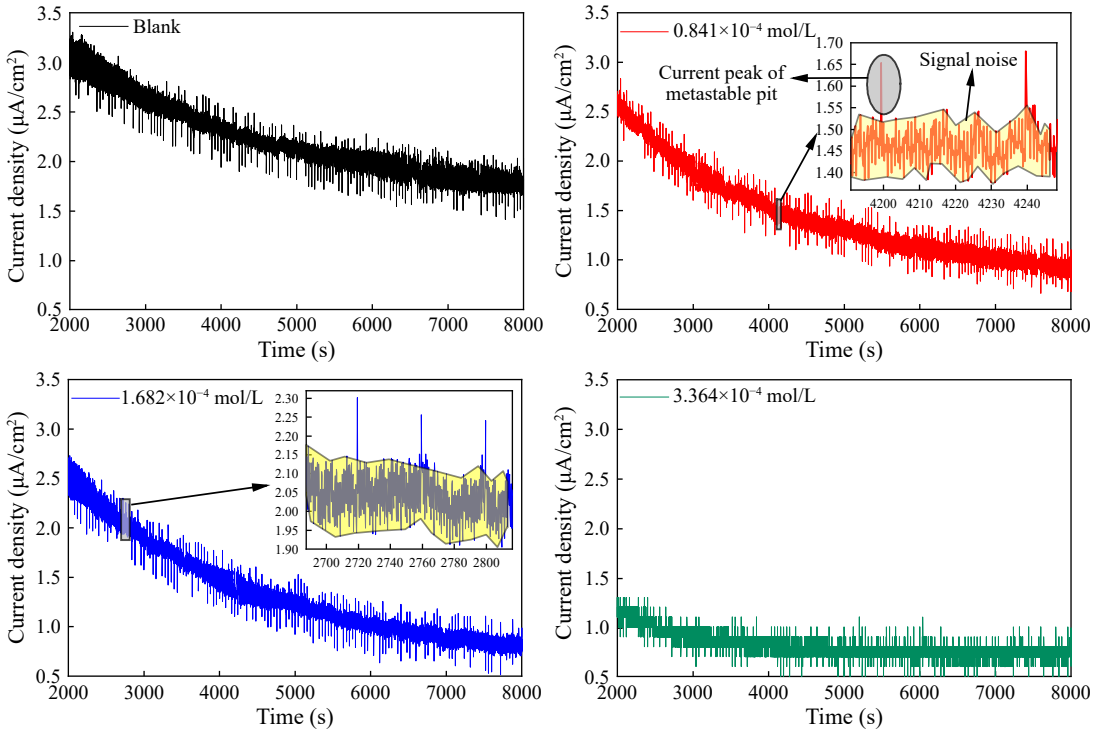

Fig.5 Typical current transients of 304SS in the SCPS with different TDS concentrations.

ing area of the specimen when the passive film has fully covered the working area, that is, the current density maintained at a steady state (Yang, 2017). As concentration of TDS increased, the current density decreased, indicating a reduction in passive film dissolution rate.

3.3 Statistical Characteristics of Metastable Pit

To analyze the distribution of the maximum depth of pits, the Gumbel extreme value distribution was applied, as follow:

$$P(x \le d_{\max}) = \exp\{-\exp[-(d_{\max} - x_{\max})/\bar{x}]\}, \quad (4)$$

where x is the random variables of maximum depth of pits. $x_{\max}$ is the depth of pits with the highest probability density, and $\bar{x}$ is the average depth of pits. In this study, seven statistical characteristics parameters were studied, which are peak current density (i_{peak}), radius of metastable pit (r_{pit}), stability product of pit ($i{\cdot}a$), growth time of metastable pit (t_{grow}), repassivation time of metastable pit (t_{rep}), growth rate of metastable pit (K_{grow}) and repassivation rate of metastable pit (K_{rep}).

3.3.1 Peak current density

The possibility of forming stable pit from metastable pit increased with i_{peak}, and extreme value distribution of pit depth can be expressed in terms of i_{peak} (Feng *et al.*, 2018):

$$P(x \le i_{\text{peak}}) = \exp\left\{-\exp\left[-(i_{\text{peak}} - x_{\max})/\alpha\right]\right\}, \quad (5)$$

where $x_{\max}$ is the metastable peak current density with the highest probability of occurrence, which indicated the value of current peak when $-\ln(\ln(1/P))$ was equal to zero. α is a scale parameter which is the reciprocal slope of the probability lines.

As the time interval has little effect on extreme value distribution of the peak current density (Wang, 2013), the current transient of the potentiostatic polarization curve was divided into 9 segments, and the maximum peak current density in each segment is investigated, and then numbered according to the value from 1 to 9. The statistical probability of the maximum peak current was calculated by Eq. (6):

$$P_j = \frac{j}{N+1}, \quad (6)$$

where N=9, and j is serial number of the corresponding maximum peak of current density.

In Fig.6, extreme value distribution of i_{peak} in the SCPS is shown for various TDS concentrations. A decrease in i_{peak} from 0.37 to 0.29 μA/cm² was observed with the addition of corrosion inhibitors, as the TDS concentrations

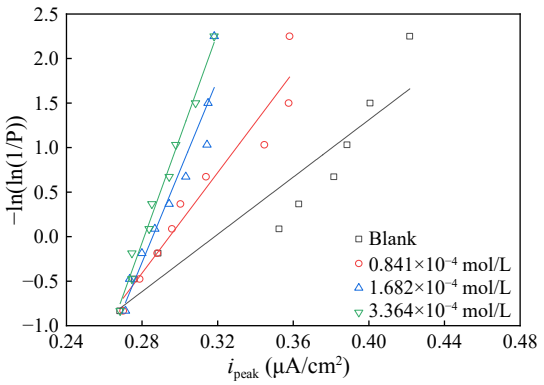

Fig.6 Extreme distribution of i_{peak} for 304SS in the SCPS with different TDS concentrations.

increased to 3.364×10^{-4} mol/L, indicating that the corrosion inhibitor reduced the formation possibility from metastable pit to stable pitting.

3.3.2 Radius of metastable pit

On the basis of hemispherical metastable pit, r_{pit} was determined in accordance with the Faraday equation as follows (Feng *et al.*, 2018):

$$r_{\mu}=\left[\left(\frac{3Z}{2\pi nF\rho}\right)\int_{t_0}^{t_1}(i_{max}-i_{bg})\,dt\right]^{\frac{1}{3}}, \quad (7)$$

where Z is the molar mass of the material, 55.2 g/mol. The mean oxidation state of the cations (n) equals to 2.19 (Aghuy *et al.*, 2015). F represents the Faraday constant. ρ is the mean density of the material, 7.93 kg/m^3.

A comparison of extreme distributions of r_{pit} in the SCPS for 304SS at different TDS concentrations is displayed in Fig.7. The values of r_{pit} decreased with increasing TDS concentration, confirming the inhibition influence of TDS on the development of the radius r_{pit}.

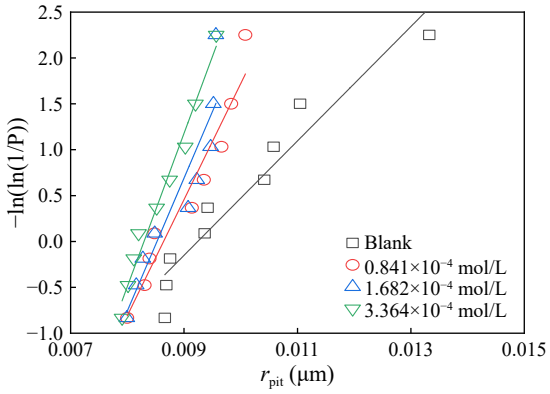

Fig.7 Extreme distribution of r_{pit} for 304SS in the SCPS with different TDS concentrations.

3.3.3 Stability product

In order to estimate the propensity of pitting transmission from the metastable state to steady state, the stability product (i·a) is calculated by taking the current density (i) and the metastable pit depth (a) (Feng *et al.*, 2018). The metal surface may become corroded due to localized defects as well as corrosion caused by corrosive medium in the surrounding environment, the generation of pitting may gradually evolve from pitting initiation to propagation. Normally, pitting will produce a covering layer to prevent the diffusion process, namely the transport of metallic cations from the pit cavity. However, the development of metastable pit would rupture the covering layer, and intensify the anodic reaction, when the stability product (i_{peak}·r_{pit}) exceed a threshold value of 3 mA·cm^{-1} (Feng *et al.*, 2018), the metastable pit would turn into the stable pitting. On the other hand, repassivation of the metastable pit may occur if the cover layer is not ruptured. In this paper, the shape of the metastable pit is assumed as hemispherical, and the pitting depth (a) is equal to the radius of metastable pit (r_{pit}). Therefore, the stability product (i·a) was expressed as i_{peak}·r_{pit}, which were calculated by metastable pit radius and peak current density.

Fig.8 represents extreme value distribution of i_{peak}·r_{pit} of 304SS. The values of i_{peak}·r_{pit} were much lower than the threshold value (3 mA/cm), indicating that the metastable pits were repassivated. Moreover, the SCPS with 3.364×10^{-4} mol/L TDS exhibited the smallest stability products with a median value reaching 0.0025 μA/cm. This further confirmed that the metastable pit was repassivated in the SCSP with a high level of TDS concentration.

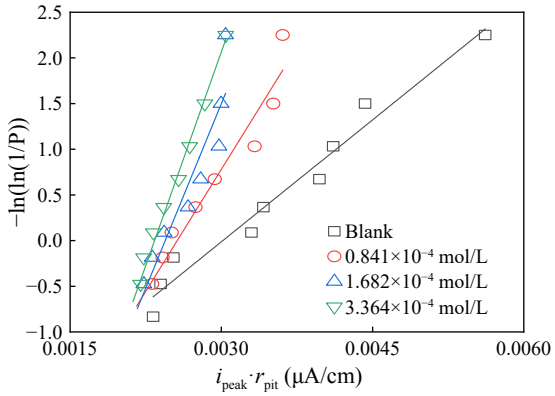

Fig.8 Extreme distribution of stability product of metastable pit for 304SS in the SCPS with different TDS concentrations.

3.3.4 Evolution on metastable growth and repassivation

Extreme value distribution of metastable life time is shown in Fig.9, and Fig.10 illustrated extreme value distribution of a total four parameters: growth time of metastable pit (t_{grow}), repassivation time of metastable pit (t_{rep}), growth rate of metastable pit (K_{grow}), and repassivation rate of metastable pit (K_{rep}).

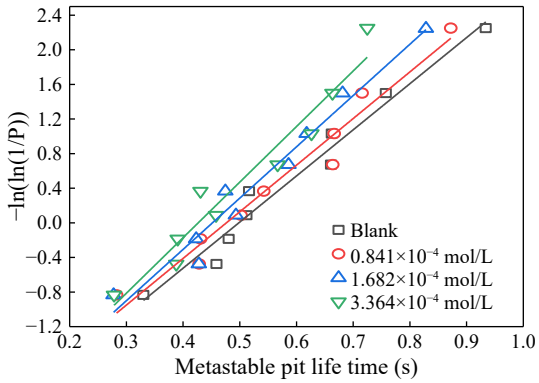

Fig.9 Extreme distribution of metastable pit life time for 304 stainless steel in the SCPS with different TDS concentrations.

All the statistical parameters of time, including life time, t_{grow} and t_{rep} decreased with the TDS concentrations as depicted in Fig.8 and Fig.9. Besides, K_{grow} and K_{rep} decreased as well. According to the analysis of the N 1s and S 2p spectra in our previous research, the adsorption mechanism was mainly attributed to the R-HSO$_3$ and trimethylamine function groups in the TDS molecular

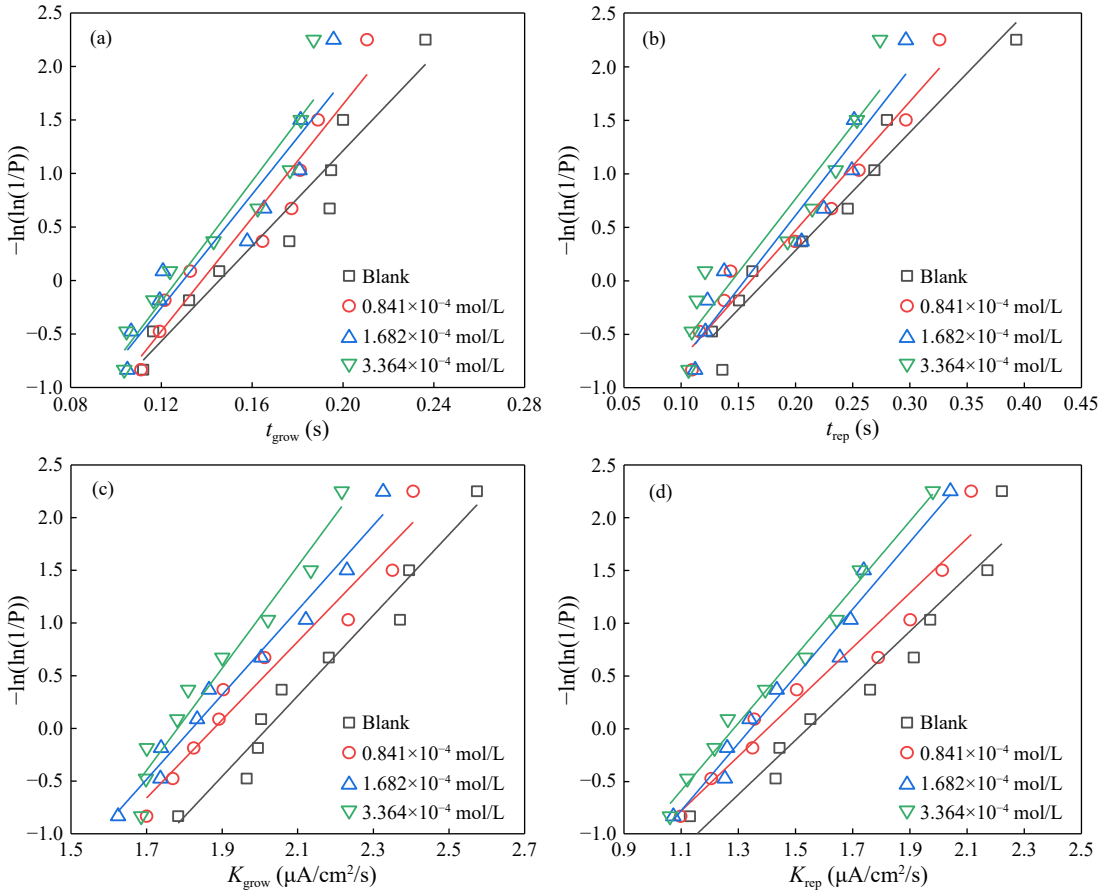

Fig.10 Extreme value distribution of metastable pits in the SCPS with different TDS concentrations. (a), growth time; (b), repassivation time; (c), growth rate; (d), repassivation rate.

(Zhao *et al*., 2019). In the SCPS, the adsorption film of TDS molecular protects the 304SS from chloride attack. Therefore, the K_{grow} decreased as a result of the addition of TDS. As mentioned before, the transfer process from metastable into stable state is closely coordinated with the rupture of cover layer. Additionally, the TDS film adsorbed on the stainless steel also prohibited the contact between the alkaline cations in the SCPS and 304SS, which slowed down the K_{rep} of the metastable pits. Analogously, aluminum tripolyphosphate has been investigated as an inhibitor of pitting, and Lu *et al*. (2019) found that addition of aluminum tripolyphosphate suppressed both K_{grow} and K_{rep}. The decreasing tendency of these parameters denoted that the addition of TDS inhibited the growth of the metastable pits, which is in accordance with the previous study by Yang *et al*. (2012), who found that corrosion inhibitors could suppress the initiation and growth of pits on steel rebar surfaces.

3.4 Mott-Schottky Diagram

In Fig.11, the Mott-Schottky diagram for 304SS in the SCPS containing a variety of TDS concentrations is shown. When the potential is below 0.58 V_{SCE}, several unobvious negative slopes can be observed, indicating this passive film is a p-type semiconductor, the acceptor density (N_A) of the passive film can be computed from these negative slopes. The positive slopes are detected in the

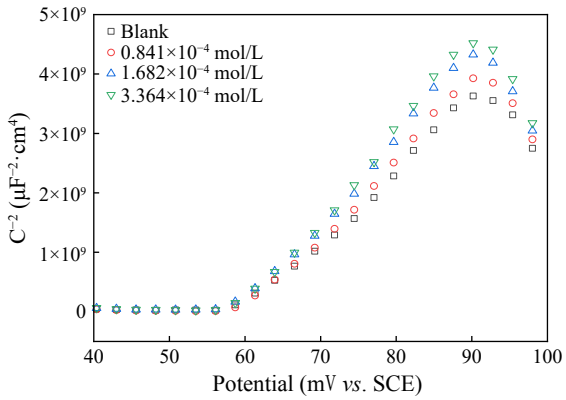

Fig.11 Mott-Schottky diagram of 304SS after 2 h immersion in the SCPS with different TDS concentrations.

potential range of 0.058 V_{SCE} to 0.090 V_{SCE}, which means that at this potential range the passive film is n-type (Vignal *et al*., 2002; Feng *et al*., 2016), also the donor density (N_D) of the passive film can be calculated from these positive slopes. Negative slopes occurred again when the applied potential exceeded 0.09 V_{SCE}, implying that the passive film had begun to breakdown (Vignal *et al*., 2002).

The calculation of space charge layer capacitance (C_{SZ}) is as follow (Dong *et al*., 2011):

$$C_{sz} = -\frac{1}{\omega Z''}, \tag{8}$$

where ω means the angular frequency, which equals to $2\pi f$. Z'' means the imaginary part of the electrochemical impedance spectroscopy.

The Mott-Schottky equation is expressed as follows (Yang *et al*., 2021):

$$\frac{1}{C_{SC}^2}=\frac{2}{eN_D\varepsilon_0\varepsilon_r}\left(E_m-E_{fb}-\frac{kT}{e}\right), \tag{9}$$

$$\frac{1}{C_{SC}^2}=\frac{2}{eN_D\varepsilon_0\varepsilon_r}\left(E_m-E_{fb}+\frac{kT}{e}\right), \tag{10}$$

where the electron charge (e) equals to 1.602×10^{-19} C, the permittivity of free space charge (ε_0) equals to 8.85×10^{-14} F/cm, and the dielectric constant of passive film (ε_r) is taken to be 15.6 (Huang *et al*., 2022). E_m means the potential of electrode, and E_{fb} means the potential of flat band. The Boltzman constant (k) equals to 1.38×10^{-23} J/K, T represents temperature, assuming the temperature is constant, kT/e is negligible since it is merely 25 mV at ambient temperature. During the analysis, it is generally presumed that the double-layer capacitance, also known as Helmholtz capacitance, is significantly greater than the capacitance of space charge layer.

Table 2 shows the donor density (N_D) calculation results, N_D reduced with increasing TDS concentrations from 9.284×10^{22} cm^{-3} to 6.927×10^{22} cm^{-3}. The reason could be related to TDS molecules adsorbing onto the passive film, thereby leading to the reduction of the Helmholtz capacitance (Feng *et al*., 2017). Meanwhile, the lower the N_D, the more stable the passive film in the SCPS, and the less sensitive to pitting (Niu, 2014).

Table 2 Effect of TDS concentration on N_D in the passive film formed after immersion for 2 h

Concentration (mol/L)	N_D (10^{22} cm^{-3})	Slope (10^8)	Intercept (10^9)	R^2
–	9.284	0.973	−5.668	0.993
0.841×10^{-4}	8.184	1.104	−6.498	0.992
1.682×10^{-4}	7.342	1.231	−7.161	0.991
3.364×10^{-4}	6.927	1.305	−7.621	0.993

Base on the study of Hamadou *et al*. (2010), the thickness of the space charge layer (W) was further calculated as follows:

$$W=\left[\frac{2\varepsilon\varepsilon_0}{eN_D}\left(E_m-E_{fb}-\frac{kT}{e}\right)\right]^{\frac{1}{2}}. \tag{11}$$

Figure 12 illustrates the values of W that formed on the surface of 304SS based the amount of TDS added. The values of W increased with the higher TDS concentrations, which indicated that the inclusion of TDS promoted the creation of thicker space charge layers on the 304SS surfaces. Therefore, the passivity of the 304SS in the SCPS was enhanced with the increase of TDS concentrations.

3.5 AFM Observation

AFM is an effective tool to investigate the localized corrsion. The AFM images of 304SS after potentiostatic polarization are illustrated in Fig.13. Obvious morphology of corrosion pit can be observed on the sample surface when the concentration of TDS is less than 0.841×10^{-4} mol/L in the SCPS, and the depth of pit is decreased from −2.2 to −0.26 μm due to the addition of TDS. However, the sample soaked in the SCPS with 1.682×10^{-4} mol/L TDS, no corrosion pitting was detected on sample surface, but the passive film was ruptured, this indicated that the existed TDS enhanced the stability of the passive film. In Fig.13(d), the 304SS surface was intact without broken, which further proved that the addition of TDS prohibited the generation of metastable pit on the 304SS.

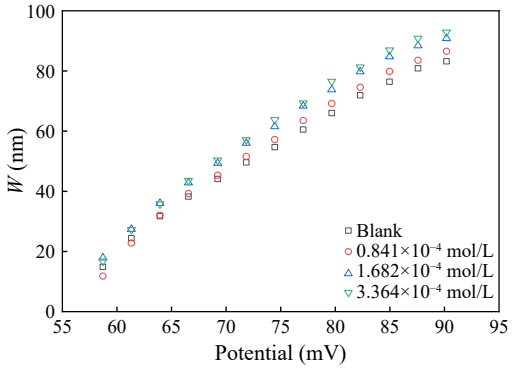

Fig.12 W of 304SS after 2 h immersion in the SCPS with different TDS concentrations.

The schematic illustration of TDS inhibition mechanism on the evolution of metastable pit is shown in Fig.14. Figures 14(d)–(f) show the evolution of metastable pit in the presence of TDS. In the highly alkaline SCPS, a passive film was formed on 304SS, and TDS adsorbed on the surfaces would prohibited the active sites from the attack of the chloride ions. The XPS analysis in our previous research demonstrated that the adsorption action is mainly caused by the R-HSO_3 and trimethylamine function groups in the TDS molecular (Zhao *et al*., 2019). The TDS adsorption film in the vicinity of the corrosion pits maybe gradually destroyed with the continuous attack of the chloride ions. However, the radius and depth of the pitting pits still decreases significantly, and the stable pitting products are reduced as well, as indicated in Figs.5–7. It is argued by Feng *et al*. (2018) that highest peak of current density mainly controls the migration of pitting from metastable state to steady state. The added TDS in this study contributed to the reduction of i_{peak}, displaying that TDS could control the transformation of metastable pits to stable pits as i_{peak} decreased with the increase in TDS concentrations.

4 Conclusions

The electrochemical measurements and AFM observations of 304SS in the SCPS with different TDS concentrations were used to examine its metastable pit characteristics in this study, and below conclusions were drawn:

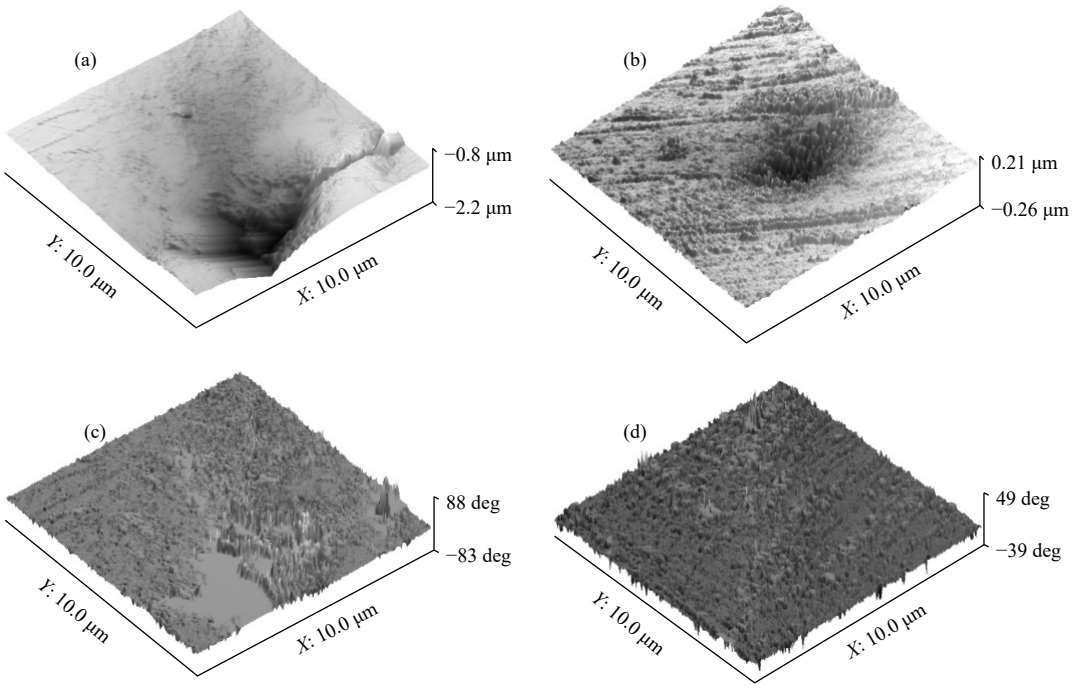

Fig.13 AFM observations on the 304SS after potentiostatic polarization in the SCPS with different TDS concentrations. (a), blank; (b), 0.841×10^{-4} mol/L; (c), 1.682×10^{-4} mol/L; (d) 3.364×10^{-4} mol/L.

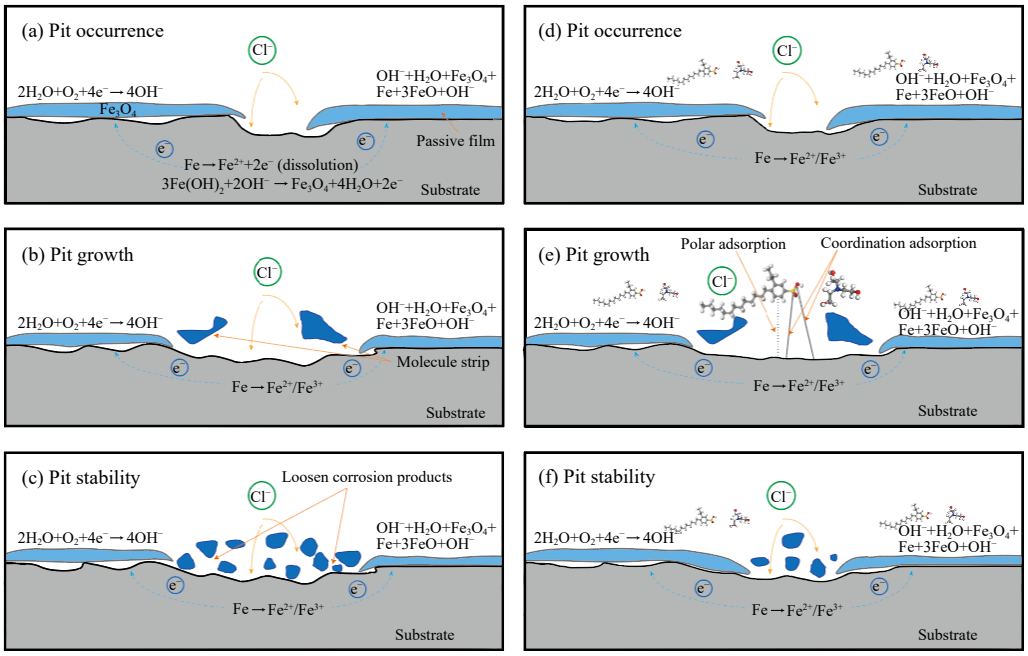

Fig.14 Schematic illustration of TDS adsorption film on the evolution of metastable pit.

1) The potentiodynamic polarization curves of 304SS demonstrated that both E_{corr} and E_b increased as TDS concentrations increased, it means that the passive film is tougher to be destroyed, and the metastable pit is more difficult to transform into stable pitting.

2) The statistical characteristics of metastable pit demonstrated that as the TDS concentrations in the SCPS increased, all seven parameters of metastable pit decreased. Theses seven parameters include i_{peak}, r_{pit}, $i_{peak}\cdot r_{pit}$, t_{grow}, t_{rep}, K_{grow} and K_{rep}. Based on these results, it appears that TDS can inhibit the sprouting and growth of metastable pit.

3) The Mott-Schottky tests showed that with increasing TDS concentrations, N_D of the passive film dropped while W increased, indicating that a higher TDS concentration in the SCPS leads to a better stability of the generated passive film, which in turn helps prevent pitting corrosion from occurring. This work recommends the use of TDS in the engineering at a concentration of not less than 3.364×10^{-4} mol/L.

Acknowledgements

The authors gratefully acknowledge the financial supports from the National Natural Science Foundation of China (Nos. 51509081, 52208241).

Author Contributions

Yingdi Liao: conceptualization, methodology, funding acquisition, supervision. Huan Zhang: investigation, writing–original draft. Xin Wang: writing–review and editing. Li Chen: investigation. Chenggeng Huang: data curation. Yazhou Zhao: writing–review and editing, formal analysis. Bo Da: conceptualization, writing–review and editing, supervision. All authors read and approved the final manuscript.

Data Availability

The data that support the findings of this study are available from the corresponding author upon reasonable request.

Declarations

Ethics Approval and Consent to Participate

This article does not contain any studies with human participants or animals performed by any of the authors.

Consent for Publication

Informed consent for publication was obtained from all participants.

Conflict of Interests

The authors declare that they have no conflict of interests.

References

Abass, A. O., 2018. Recent advances on organic coating system technologies for corrosion protection of offshore metallic structures. *Journal of Molecular Liquids*, **269**: 572–606.

Aghuy, A., Zakeri, M., Moayed, M. H., and Mazinani, M., 2015. Effect of grain size on pitting corrosion of 304L austenitic stainless steel. *Corrosion Science*, **94**: 368–376.

Chen, D., Zhang, P. C., Pan, T., Liao, Y. D., and Zhao, H., 2019. Evaluation of the eco-friendly crushed waste oyster shell mortars containing supplementary cementitious materials. *Journal of Cleaner Production*, **237**: 117811.

Da, B., Yu, H. F., Ma, H. Y., Tan, Y. S., Mi, R. J., and Dou, X. M., 2016. Chloride diffusion study of coral concrete in a marine environment. *Construction and Building Materials*, **123**: 47–58.

Dong, Z., Shi, W., Zhang, G., and Guo, X., 2011. The role of inhibitors on the repassivation of pitting corrosion of carbon steel in synthetic carbonated concrete pore solution. *Electrochimica Acta*, **56** (17): 5890–5897.

Feng, X., Lu, X., Zuo, Y., Zhuang, N., and Chen, D., 2016. The effect of deformation on metastable pitting of 304 stainless steel in chloride contaminated concrete pore solution. *Corrosion Science*, **103**: 223–229.

Feng, X., Shi, R., Lu, X., Xu, Y., Huang, X., and Chen, D., 2017. The corrosion inhibition efficiency of aluminum tripolyphosphate on carbon steel in carbonated concrete pore solution. *Corrosion Science*, **124**: 150–159.

Feng, X., Xu, Y., Zhang, X., Lu, X., Zhang, L., Shi, R., *et al*., 2018. A statistical study on metastable pitting of 304 stainless steel in chloride contaminated carbonated concrete pore solution. *International Journal of Electrochemical Science*, **13**: 10339–10354.

Haleem, S. M., Wanees, S., Aal, E. E., and Diab, A., 2010. Environmental factors affecting the corrosion behavior of reinforcing steel II. Role of some anions in the initiation and inhibition of pitting corrosion of steel in $Ca(OH)_2$ solutions. *Corrosion Science*, **52** (2): 292–302.

Hamadou, L., Kadri, A., and Benbrahim, N., 2010. Impedance investigation of thermally formed oxide films on AISI 304L stainless steel. *Corrosion Science*, **52**: 859–864.

Huang, L., Chang, W., Zhang, D., Huang, Y., Li, Z., Lou, Y., *et al*., 2022. Acceleration of corrosion of 304 stainless steel by outward extracellular electron transfer of *Pseudomonas aeruginosa* biofilm. *Corrosion Science*, **199**: 110159.

Liao, Y. D., Fan, J. H., Li, R. N., Da, B., Chen, D., and Zhang, Y., 2022. Influence of the usage of waste oyster shell powder on mechanical properties and durability of mortar. *Advanced Powder Technology*, **33**: 103503.

Lu, X., Zhang, L., Feng, X., Chen, D., and Zuo, Y., 2019. Effect of aluminum Tripolyphosphate on pitting initiation on carbon steel in chloride contaminated concrete pore solution. *Anti-Corrosion Methods and Materials*, **66**: 603–612.

Naghizadeh, M., Nakhaie, D., Zakeri, M., and Moayed, M. H., 2015. The effect of dichromate ion on the pitting corrosion of AISI 316 stainless steel Part II: Pit initiation and transition to stability. *Corrosion Science*, **94**: 420–427.

Niu, B., 2014. The effect of NO_2^- on the pitting corrosion of Q235 carbon steel in synthetic carbonnated concrete p.. PhD thesis. Beijing University of Chemical Technology, Beijing.

Shi, J. S., Liu, C., Wang, D. F., Liu, Z. Y., Liu, G. J., Chun, Q., *et al*., 2023. Numerical simulation of effective diffusivity in concrete with random microcracks. *Journal of Building Engineering*, **63**: 105501.

Tian, H., Fan, L., Li, Y., Pang, K., Chu, F., Wang, X., *et al*., 2021. Effect of NH_4^+ on the pitting corrosion behavior of 316 stainless steel in the chloride environment. *Journal of Electroanalytical Chemistry*, **894**: 115368.

Vignal, V., Valot, C., Oltra, R., Verneau, M., and Coudreuse, L., 2002. Analogy between the effects of a mechanical and chemical perturbation on the conductivity of passive films. *Corrosion Science*, **44**: 1477–1496.

Wang, D., Ming, J., and Shi, J., 2020. Enhanced corrosion resistance of rebar in carbonated concrete pore solutions by Na_2HPO_4 and benzotriazole. *Corrosion Science*, **174**: 108830.

Wang, Y. Y., 2013. Research on the early current fluctuation of pitting corrosion. PhD thesis. Beijing University of Chemical Technology, Beijing.

Yang, G., Du, Y., Chen, S., Ren, Y., and Ma, Y., 2021. Effect of secondary passivation on corrosion behavior and semiconducting properties of passive film of 2205 duplex stainless steel. *Journal of Materials Research and Technology*, **15**: 6828–6840.

Yang, K. J., 2017. Preparation and surface modification of the

high entropy alloy/nitride co-deposition coating for stainless steel bipolar plate. PhD thesis. Lanzhou University of Technology, Lanzhou.

Yang, R. J., Guo, Y., Tang, F., Wang, X., Du, R., and Lin, C., 2012. Effect of sodium D-gluconate-based inhibitor in preventing corrosion of reinforcing steel in simulated concrete pore solutions. *Acta Physico-Chimica Sinica*, **28**: 1923–1928.

Zhang, M., and Long, Y., 2010. Inhibition of triethanolamine for magnetic refrigeration material $LaFe_{11.0}Co_{0.7}Si_{1.3}$ in distilled water. *The 7th National Conference on Functional Materials and Applications*. Changsha, China.

Zhao, Y. Z., Chen, Y., Li, X. Y., Chen, D., and Wu, M., 2023. The use of TEA·H_3PO_4 and TEA·$C_{18}H_{30}O_3S$ as eco-friendly corrosion inhibitors in cementitious materials: An experimental and theoretical study. *Cement and Concrete Research*, **165**: 107073.

Zhao, Y. Z., Pan, T., and Yu, X. T., 2019. Corrosion inhibition efficiency of triethanolammonium dodecylbenzene sulfonate on Q235 carbon steel in simulated concrete pore solution. *Corrosion Science*, **158**: 108097.

(Edited by Ji Dechun)